nature communications

Article

https://doi.org/10.1038/s41467-025-66924-0

A practical method for determining the rate of covalent modification of fragments and leads

Received: 17 March 2025

Accepted: 17 November 2025

Published online: 18 December 2025

Check for updates

Janice Jeon[1], Svetlana A. Kholodar[1], Brian H. Tran[1], Kimberly E. Mallinger[1], Daniel A. Erlanson[1] & Robert A. Everley[2]

The clinical success of covalent drugs such as sotorasib has renewed interest in covalency for rational drug design. The most rigorous potency metric for covalent modifiers is the second-order rate constant k_{inact}/K_I. However, existing methods for measuring k_{inact}/K_I are resource-intensive and involve complex data interpretation. We describe the diagonal dose-response time-course (dDRTC), an efficient mass spectrometry-based method for determining k_{inact}/K_I, enabling routine k_{inact}/K_I quantification earlier in programs and accelerating SAR interpretation for lead discovery. We apply dDRTC to a dozen covalent fragment and lead-like modifiers for three targets, $KRAS^{G12C}$ and two E3 ligase complexes. Kinetic simulations comparing a range of k_{inact} and K_I values establish recommended parameters for dDRTC and reveal that the approach is particularly suited for covalent fragments and leads. Our results demonstrate accurate determination of k_{inact}/K_I values across three orders of magnitude with eight-fold increased throughput, reduced protein consumption, and simplified data analysis.

Over the past decade, covalent drug discovery has undergone a surge of interest driven by the approvals of targeted covalent drugs and the rise of technological advancements accelerating covalent drug development. Previous safety concerns about off-target reactivity and toxicity steered researchers away from covalent mechanisms[1]. However, covalent inhibitors such as ibrutinib and osimertinib have achieved impressive efficacy and safety in patients with durable engagement of their targets. Moreover, the discovery of $KRAS^{G12C}$ covalent inhibitors reveals the potential of covalency to target traditionally undruggable proteins with shallow pockets[2,3]. Ibrutinib and most other targeted covalent inhibitors were developed by grafting an electrophile onto a known high-affinity ligand. Building on a disulfide-based tethering method of fragment discovery[4], a newer electrophile-first approach starts with small fragments capable of forming covalent bonds with proteins to identify weak modifiers that are subsequently optimized. This fragment-based approach was used in the discovery of sotorasib and covalent inhibitors for other targets beyond KRAS[5–12].

In covalent hit-to-lead cascades, mass spectrometry (MS) often plays an instrumental role by enabling direct detection of covalent protein-ligand adducts. MS does not require a competitive probe and is not limited to functional binding events. Thus, MS can be used in programs targeting poorly characterized proteins with no existing chemical probes and can be used to develop site-specific ligands that bind at sites that are non-functional, as is the case for finding novel binders to E3 ligases. In addition, compared to fluorescence or luminescence readouts, MS is less susceptible to interference and false positives[13]. MS can also determine binding stoichiometry and confirm sites of modification using enzymatic cleavage or top-down MS/MS[14].

Intact protein MS (iMS) is frequently employed to screen electrophilic fragment libraries and characterize covalent modifiers in dose-response (DR) and time-course (TC) format[12,15]. iMS is commonly performed via liquid chromatography coupled to MS (LC-MS), though the practical utility of conventional LC-MS workflows has been limited by modest sample throughput. Pairing Time-of-Flight (ToF) MS with an

[1]Frontier Medicines, 151 Oyster Point Blvd., 2nd Floor, South San Francisco, CA 94080, USA. [2]Frontier Medicines, 451 D. St., 2nd Floor, Boston, MA 02210, USA. e-mail: robert.everley@frontiermeds.com

Agilent RapidFire system improves acquisition time from minutes to seconds[16], and additional analytical advancements have led to techniques such as infrared matrix-assisted laser desorption electrospray ionization (IR-MALDESI), with reported sample rates as high as 1.5–22 Hz[17].

Despite the advantages of MS for covalent drug discovery, full characterization of the potency of covalent compounds involves characterizing both time- and dose-dependent behavior, which can be resource-intensive. For reversible drugs, equilibrium constants (K_D) or IC_{50} values are often used to drive SAR. However, the time-dependent mechanism of irreversible modifiers makes IC_{50} values inadequate; an IC_{50} measurement taken at five minutes might be very different from one taken at two hours, and multiple researchers have written of the limitations of relying on IC_{50} alone to guide SAR[18–20]. A more rigorous assessment of irreversible modifiers is the ratio k_{inact}/K_I, a time- and concentration-independent inactivation rate constant that incorporates a covalent modifier's reactivity towards the target (k_{inact}) and factors influencing k_{inact}, as well as its reversible affinity (K_I)[14–16].

Irreversible covalent binding occurs in two steps as described in Eq. (1), where P, L, P:L, and PL denote protein, ligand, noncovalent binary complex, and covalent binary complex, respectively.

$$P + L \overset{K_I}{\rightleftharpoons} P:L \xrightarrow{k_{inact}} PL \tag{1}$$

k_{inact}/K_I allows for the relative ranking of covalent binding efficiencies, even with low reversible affinity[21]. It is also the preferred means of predicting in vitro and in vivo target occupancy and therapeutic effect[20]. Furthermore, the ratio has demonstrated greater accuracy in predicting drug-drug interactions and off-target effects compared to IC_{50}[22,23]; guidance from the U.S. Food and Drug Administration and European Medicines Agency now advises investigating the inhibition mechanism and inactivation kinetics to evaluate the risk of drug-drug interactions[24,25].

MS-enabled programs traditionally obtain k_{inact}/K_I values with a full iMS DRTC, a resource-intensive experiment involving a two-dimensional matrix varying time on one axis and dose on the other, leading to a sample size of n doses multiplied by n time points for a single compound. After measuring occupancy across a range of time points, the observed rate of inactivation (k_{obs}) values estimated with Eq. (2) can be plotted as a function of inhibitor concentration and fit to determine k_{inact}/K_I with Eq. (3).

$$\%\text{Total Occupancy} = 100\left(1 - e^{-k_{obs}t}\right) \tag{2}$$

$$k_{obs} = \frac{k_{inact}[L]}{K_I + [L]} \tag{3}$$

Unfortunately, despite offering the most accurate determination of covalent potency, a full DRTC is not practical as a weekly SAR tool due to the protein consumption, instrument time, and complicated data analysis involved; a typical SAR campaign with around 35 compounds a week would require six 384-well plates for a full 8 × 8 DRTC because a single 384-well plate can accommodate only six compounds in this format.

Here, we report a practical alternative: the diagonal DRTC (dDRTC) method, which provides accurate measurement of k_{inact}/K_I and is sufficiently high-throughput for routine SAR for a hit-to lead optimization campaign. The number of samples is reduced from n x n samples for a full checkerboard down to just n samples in the diagonal slice, which is the same number of samples as a conventional IC_{50} experiment. Moreover, dDRTC data analysis can easily be automated by applying standard curve-fitting approaches commonly used during SAR campaigns. The method also provides superior coverage of dose-time space compared to DR or TC under the same assay conditions, and this expanded dynamic range offers valuable positive and negative SAR insights to medicinal chemists.

In this work, we acquire iMS data in both the traditional full DRTC and dDRTC format for twelve covalent fragments and lead-like modifiers of $KRAS^{G12C}$ and previously unliganded E3 ligase complexes, SKP1-FBXW7 and SOCS2-EloB-EloC. In addition, we run dozens of simulations in KinTek Global Kinetic Explorer[26] for a range of k_{inact} and K_I values to understand the optimal conditions where the dDRTC method delivers accurate and reliable k_{inact}/K_I values. Our results demonstrate reproducible, quantitative determination of k_{inact}/K_I values over more than three orders of magnitude while using eight-fold fewer resources, including both time and reagents.

Results

We sought to develop a streamlined method for obtaining k_{inact}/K_I that would be more amenable to routine SAR studies compared to a full DRTC. Our aim was to use a common DR curve format with the y-axis as our measurement (% occupancy quantified by iMS) and the x-axis with the units of the desired endpoint of k_{inact}/K_I ($M^{-1}s^{-1}$) and utilize only the diagonal slice of the checkerboard (Fig. 1). This approach is related to drug combination and drug synergy screens, where checkerboards are used to compare a dose range of one drug vs. another; the diagonal slice of a full checkerboard is the most informative sample of the checkerboard[27,28].

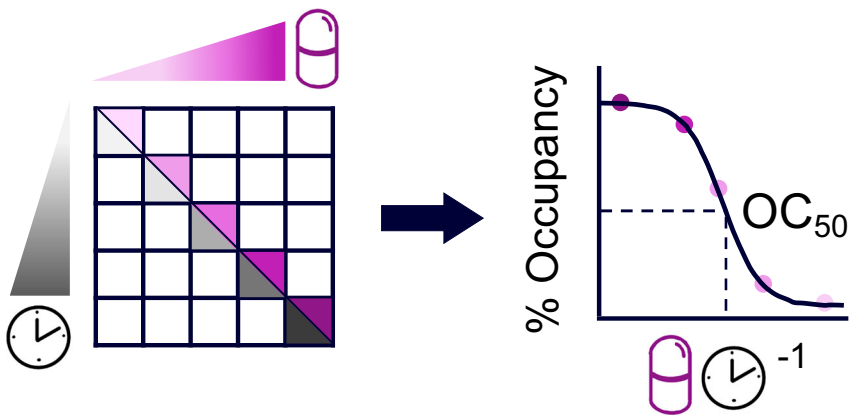

Fig. 1 | A schematic representation of the diagonal dose-response time-course (dDRTC) method to determine k_{inact}/K_I. For an n x n checkerboard with varying time on one axis and varying dose on another, only the diagonal sampling (in color) is measured. After testing samples in intact protein MS, an occupancy curve can be fit to determine OC_{50}, the dose and time which yields 50% occupancy, which is then converted to k_{inact}/K_I. Y = % occupancy, and X = the inverse product of dose and time in units of k_{inact}/K_I ($M^{-1}s^{-1}$).

Derivation of the relationship between OC_{50} and k_{inact}/K_I

We sought to provide the theory to justify the dDRTC approach and derive a relationship between OC_{50} and k_{inact}/K_I both in units of ($M^{-1}s^{-1}$). Building on derivations by Copeland et al.[29], we established a relationship between OC_{50} and k_{inact}/K_I beginning with the following pseudo first-order rate Eq. (4) under the assumption [L] > [P], which generally holds true in the early stages of covalent drug discovery where protein concentrations are typically 1 μM or less:

$$[PL]_t = [PL]_{eq}\left(1 - e^{-k_{obs}t}\right) \tag{4}$$

$[PL]_t$ is the %PL (i.e., covalent occupancy) at time t and $[PL]_{eq}$ is 100% maximum occupancy. We converted Eq. (4) as follows:

$$\%PL_t = 100\left(1 - e^{-k_{obs}t}\right) \tag{5}$$

With $k_{obs} = \frac{k_{inact}[L]}{K_I + [L]}$ from Eq. 3,

$$\%PL_t = 100\left(1 - e^{-\frac{k_{inact}[L]}{K_I + [L]}t}\right) \tag{6}$$

When $[L] \ll K_I$,

$$\%PL_t = 100\left(1 - e^{-\frac{k_{inact}}{K_I}[L]t}\right) \tag{7}$$

$$e^{-\frac{k_{inact}}{K_I}[L]t} = 1 - \frac{\%PL_t}{100} \tag{8}$$

$$-\frac{k_{inact}}{K_I}[L]t = \ln\frac{100 - \%PL_t}{100} \tag{9}$$

$$\frac{k_{inact}}{K_I} = -\frac{\ln\frac{100-\%PL_t}{100}}{[L]t} \tag{10}$$

We defined the OC_{50} as an estimate of the dose and time value ($M^{-1}s^{-1}$) that yields 50% occupancy: $1/([L] \times t)_{\%PL = 50\%}$. Thus,

$$\frac{k_{inact}}{K_I} = \frac{\ln 2}{[L]t} = \ln 2 \cdot OC_{50} \tag{11}$$

Consistent with our goal of applying a streamlined method to determine the efficiency of covalent bond formation (k_{inact}/K_I) for targets beyond enzymes, the relationship described in Eq. (11) does not require knowledge of substrate concentration or K_M.

k_{inact}/K_I from diagonal sampling of the checkerboard

We designed an 8 × 8 checkerboard of time and dose conditions to assess ARS-853[30,31], a cell-active, selective, covalent $KRAS^{G12C}$ inhibitor, and prepared iMS samples according to the conditions across the diagonal slice (**Series 1** in Table 1). To obtain OC_{50}, we plotted the percentage of $KRAS^{G12C}$ bound to ARS-853 against the inverse product of time and dose (Fig. 2A) and fit the data using a commonly applied four-parameter logistic regression, where Y = % occupancy and X = the inverse product of dose and time (in units of k_{inact}/K_I) as both dose and time were varied during the study.

The average OC_{50} for ARS-853 in the dDRTC method for two independent experiments was 310 ± 10.3 $M^{-1}s^{-1}$ (mean ± SEM). Using Eq. (11) to convert the OC_{50} for ARS-853, we found that the k_{inact}/K_I of 215.0 ± 7.1 $M^{-1}s^{-1}$ from dDRTC was within 20% of the reported literature value of 250 ± 20 $M^{-1}s^{-1}$[30].

We also ran the full 8 × 8 DRTC with ARS-853 for comparison and applied a global fit according to Eqs. (2) and (3) (Fig. 2B). Global fitting ensured consistent, robust, and accurate parameter estimates by simultaneously fitting the model to all curves within the group. The average k_{inact}/K_I over two independent experiments was 274.2 ± 0.8 $M^{-1}s^{-1}$, also within 20% of the reported value.

General correlation of k_{inact}/K_I from dDRTC vs. full DRTC

Beyond the ARS-853 example, we sought to further test the agreement between a full checkerboard approach and dDRTC by comparing their respective k_{inact}/K_I values. We selected four additional covalent inhibitors of $KRAS^{G12C}$ as well as seven covalent modifiers of two E3 ligase complexes, SKP1-FBXW7 and SOCS2-EloB-EloC (Supplementary Table 1). Potencies spanned 1 to 2000 $M^{-1}s^{-1}$, covering early hit optimization into lead generation potencies and compound sizes[7]. Dose-time schemes evolve with compound potency, and we have provided general guidance for condition selection in Supplementary Table 2.

The linear regression analysis for k_{inact}/K_I determined by the full DRTC vs. dDRTC method demonstrated a near 1:1 and statistically significant relationship as well as strong correlation ($y = 0.8141x$, $p = 1.42974 \times 10^{-11}$, $R^2 = 0.9817$), indicating a high degree of alignment between methods (Fig. 3). In addition, the median percent difference ($n = 12$) between the gold-standard approach and dDRTC was 19% (Supplementary Tables 3 and 4), showing the dDRTC approach can accurately reflect k_{inact}/K_I while reducing resource (reagents and time) consumption and increasing throughput to support iterative hit-to-lead optimization campaigns.

Simulations suggest the dDRTC method is ideal for early-stage programs

To understand the applicable range where dDRTC is best suited, we simulated datasets across a broad range of k_{inact} (0.00005 − 1 s^{-1}) and K_I (1 − 1000 μM) values (see Methods/SI for details). These simulations were agnostic to the molecular weight of the compounds and the target being modified. Consistent with the assumption $K_I \gg [L]$ used in deriving the relationship between dDRTC OC_{50} and true k_{inact}/K_I (Eq. (11)), dDRTC accurately quantified k_{inact}/K_I values for covalent modifiers with low reversible affinities. The simulations did not predict significant deviation (≥ two-fold difference) for modifiers with $K_I \geq 50$ μM within the wide potency range of 1 to 10,000 $M^{-1}s^{-1}$, aligning with a typical kinetic profile for early covalent leads or compounds that are optimized for k_{inact}[32], such as sotorasib, which has a reported K_I of > 50 μM (Fig. 4)[3,33]. Improving K_I to less than 50 μM led to greater deviation between true k_{inact}/K_I and dDRTC-derived values, particularly at low k_{inact}/K_I, thus defining the utility of the dDRTC method as a highly efficient early lead discovery tool, or perhaps later in k_{inact} driven programs.

Discussion

We present a practical, resource-efficient method for estimating k_{inact}/K_I over a broad dose-time space. We applied common curve fitting techniques to the information-rich diagonal datapoints of a full DRTC checkerboard and approximated k_{inact}/K_I from OC_{50} initially with the cell-active compound ARS-853. We then extended the study to a dozen covalent modifiers spanning both fragment and beyond-rule-of-three lead-like space, for $KRAS^{G12C}$ and two E3 ligase complexes, SKP1-FBXW7 and SOCS2-EloB-EloC, for which no approved drugs exist. We analyzed the k_{inact}/K_I across more than three orders of magnitude via iMS and validated the results against the full DRTC checkerboard method, observing a strong correlation between the two methods. Kinetic simulations further highlighted the strengths of dDRTC as an early-stage tool that enables teams to obtain k_{inact}/K_I values earlier and more frequently in a drug discovery program, overcoming the resource barriers of the traditional approach.

Outside of the optimal dDRTC k_{inact} and K_I boundaries indicated by the simulations, other methods, such as a bimolecular reaction model[34] may be more appropriate for highly potent modifiers with

https://doi.org/10.1038/s41467-025-66924-0

Table 1 | Dose and time schemes for dDRTC

Series 1		Series 2		Series 3		Series 4	
Time s	Concentration μM	Time s	Concentration μM	Time s	Concentration μM	Time s	Concentration μM
15	1.65	120	1.56	112.5	0.783	60	2.5
60	1.65	360	3.13	225	1.57	300	5
120	3.8	900	6.25	450	3.13	900	10
360	5.8	1800	12.5	900	6.25	1800	15
900	10.9	3600	25	1800	12.5	7200	25
1800	25	10800	50	3600	25	21600	50
3600	57	21600	100	10800	50	72000	100
10800	85	72000	200	21600	100	–	–

Compounds 2, 3 (ARS-853), 4, and 5 (medium to high potency) were run with the **Series 1** scheme. Compound 1 (low potency) was run with the **Series 2** scheme. Compounds 6-10 were run with **Series 3**. Compounds 11 and 12 were run with **Series 4**. Rationale for dose-time schemes provided in Supplementary Table 2.

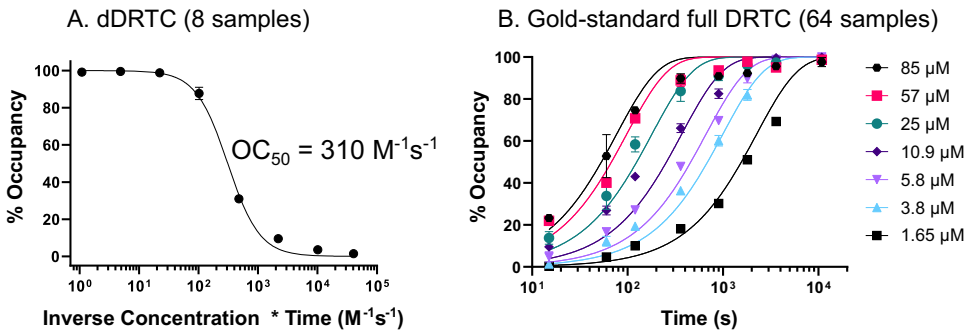

Fig. 2 | Comparison of dDRTC vs. gold-standard full DRTC checkerboard approach using KRAS^{G12C} occupancy by ARS-853 quantified via intact protein MS. Assay dose and time conditions prepared according to the **Series 1** scheme. Error bars indicate SEM. **A** OC_{50} curve from the diagonal slice of the 8 × 8 checkerboard. Each data point is the mean of two technical replicates with 8 data points per experiment. Data were fit using a common curve-fitting approach of four-parameter logistic regression. **B** Full DRTC curves with global fitting. Each data point is the mean of two technical replicates with 64 data points per experiment. Source data are provided as a Source Data file.

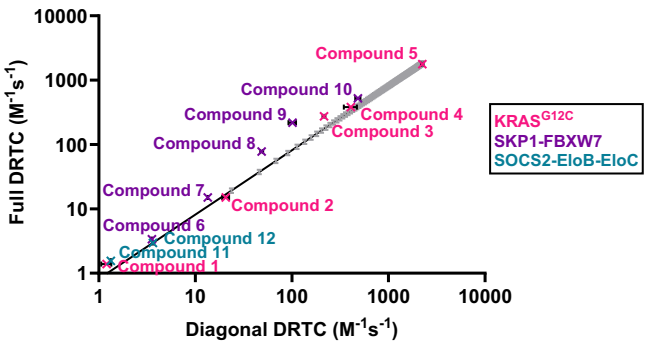

Fig. 3 | Linear regression analysis for k_{inact}/K_I determined from full DRTC vs. diagonal DRTC ($n = 12$ compounds, $p = 1.42974E\text{-}11$, $R^2 = 0.9817$). Each data point for both dDRTC and full DRTC is the mean of two technical replicates. Error bars indicate SEM, and gray shading indicates the 95% confidence interval. Source data are provided as a Source Data file.

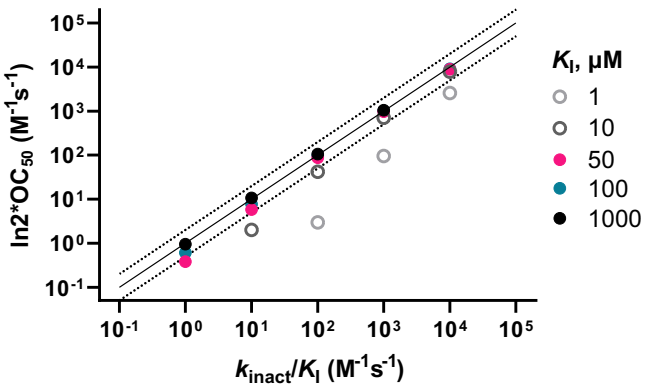

Fig. 4 | Accurate quantification of the covalent potencies (k_{inact}/K_I) by dDRTC. Simulation predicts no deviation between dDRTC OC_{50}-derived k_{inact}/K_I values $(\ln 2 \cdot OC_{50})$ plotted on the *y*-axis and true k_{inact}/K_I (x-axis) for the covalent modifiers with reversible affinities (K_I) ≥ 50 μM (filled circles). The solid line represents a perfect positive correlation where $\ln 2 \cdot OC_{50} = k_{inact}/K_I$, and the dotted lines indicate two-fold deviation margins. Optimized leads with $K_I < 50$ μM (empty circles) exhibit increasing deviation with improving reversible affinities.

$k_{inact}/K_I > 10{,}000\ M^{-1}s^{-1}$ and full DRTC or SPR analysis for leads with $K_I < 50$ μM; Compound 9 was the only compound that deviated from the full DRTC ~two-fold, and it had the lowest K_I (10 μM, Supplementary Table 5), consistent with the simulation results. In general, reaching these potencies indicates significant progress for a project team and confirmation that a protein can be targeted with covalent modifiers. At this stage, the dDRTC assay has enabled the team with suitable chemical matter for probe-competition assays, which can be used to further drive SAR and determine k_{inact}/K_I relative to the known k_{inact}/K_I of the probe (Supplementary Fig. 1)[35]. In addition, at values of $k_{inact}/K_I > \sim 400\ M^{-1}s^{-1}$, cellular activity is expected, and this becomes more important in driving further optimization[7].

Though MS is particularly well-suited for assessing covalent potency, other methods have been used to derive k_{inact}/K_I from biochemical data, including time-dependent endpoint probe competition

Table 2 | Summary of pros and cons of kinetic assays for the quantification of the rate of covalent modification, k_{inact}/K_I

Requirement	Biochemical Assays[b]	dDRTC (MS)	DRTC (MS)	SPR
Unambiguous covalent detection	No	Yes	Yes	No
Probe/functional assay	Yes	No	No	No
Protein tagging	Yes	No	No	Yes[d]
Specialized instrumentation	No	Yes	Yes	Yes
Advanced data fitting software	No	No	Yes	Yes
Throughput[a]	High	High	Low	Medium/Low[c]
Protein consumption	Low	Low	High	Low

[a]"High"-throughput, as noted here, indicates an assay that is adaptable to weekly SAR studies, whereas "Low"-throughput assays are not practical for the same purpose. [b]Examples include continuous enzymatic activity and probe competition assays. [c]Whereas SPR is considered a medium throughput method for the reversible binding examination, quantification of the irreversible binding kinetics is often associated with decreased throughput due to the surface inactivation. Regenerable SPR chip surfaces may offer improved throughput ref. 41. [d]Despite often being referred to as a label-free technique, affinity tag (e.g., Avi-tag) is often required for protein capture on the surface.

assays and pre-incubation assays such as EPIC-FIT[35,36]. However, probes may not be available for new targets, and not all covalent modifiers are amenable to functional IC_{50} shift assays that require the covalent modifier to be an inhibitor. Indeed, some covalent modifiers may not alter protein function, such as covalent ligands designed to induce proximity between two proteins, e.g., the ligands shown earlier that modify E3 ligase complexes (note: though k_{inact} may not be the most accurate term in this case as we are not inactivating the E3 ligases, for the purposes of this manuscript, we have chosen to maintain terminology commonly used in the field of covalent drug discovery). For a broader understanding of covalent occupancy's impact on function, which can differ for each target, a very helpful concept known as target vulnerability has been described[22]. To further aid the reader in positioning dDRTC as a tool in their discovery toolbox, Table 2 outlines the pros and cons of kinetic IC_{50}-based assays, iMS, and SPR, each appropriate for different experimental contexts and research goals.

iMS DR and TC assays can guide SAR in the early stages of a program, but both assays have shortcomings that can be addressed with the dDRTC method. For an iMS assay with sensitivity limits above 1 μM of protein, the effective assay range for a DR curve is the solubility limit of a compound (often 400 μM or less based on experimental measurement and in-house solubility prediction algorithms), down to a dose that maintains pseudo-first-order kinetics, i.e., [L] > [P] to allow for 100% modification. This could be addressed by digesting the protein into peptides after the reaction or concentrating the protein prior to MS, both of which could lower the starting concentration of protein required, but are beyond the scope of this manuscript. To extend the range of SAR using the DR approach, multiple incubation times are needed, and in the case of a fixed-dose TC approach, researchers are limited by practical, user-friendly considerations such as standardized time points. Thus, by modulating time and dose simultaneously, dDRTC provides SAR across a wider range of potencies under the same assay conditions (see Supplementary Fig. 2, Supplementary Fig. 3, and Supplementary Table 6) and eliminates the need to run multiple curves over a range of time points and/or doses.

Another attractive feature of dDRTC is that k_{inact}/K_I is estimated directly from the OC_{50} curve, which provides a simple, visual representation similar to more commonly used IC_{50} values. Previously reported approaches rely on correlating a value such as IC_{50} to k_{inact}/K_I and then using regression to derive k_{inact}/K_I[37–39]. As demonstrated in those studies, it would be necessary to run a full DRTC checkerboard for many compounds to establish the initial calibration curve, which may not be possible in the early stages of a program due to a lack of compounds across a wide range of potencies. The dDRTC method eliminates the need for this step.

Comparing the throughput of dDRTC and full DRTC, the dDRTC method significantly reduces protein consumption and instrument runtime and is amenable to weekly SAR, i.e., less than 100 compounds per week. An 8-point dDRTC can provide k_{inact}/K_I for 48 compounds per 384-well plate in contrast to six compounds in an 8 × 8 full DRTC. Thus, for a typical weekly SAR assay with 35 compounds, a single 384-well plate has more than enough capacity for the full set of compounds in an 8-point dDRTC format, which would require 1960 fewer samples, saving approximately 1.2 mg of protein (using KRAS as an example), compared to an 8 × 8 full DRTC. This is particularly advantageous for targets that are difficult to express. Although the full checkerboard is not practical for routine compound profiling during hit-to-lead optimization, because it is the gold standard and can discriminate k_{inact} from K_I, we recommend teams spot-check values using full DRTC when there is a ten-fold increase in potency to assess whether the lead series is still within the suggested dDRTC k_{inact} and K_I boundaries.

The dDRTC method can deliver k_{inact}/K_I values for covalent modifiers over at least three orders of magnitude of potency with an eight-fold increase in throughput by utilizing the diagonal slice of an 8 × 8 checkerboard, all with a more simplified data analysis. It can also be applied to proteins for which no previous binders or functional assays exist. dDRTC enables k_{inact}/K_I determination earlier and more frequently in a drug discovery campaign where these values can be used as a comparative metric for covalent fragments and leads through methods such as Rate Enhancement Factor analysis[21]. Our simulations extend the characterization of the dDRTC method and provide guidelines for implementation according to the stage of a program. We routinely use dDRTC at Frontier Medicines to profile our compounds, and we believe this method will help others in covalent fragment drug discovery accurately define inactivation kinetics on a scale amenable for SAR studies.

Methods

The compounds in this study were selected from our internal library as well as published compounds. While Compound 3 (ARS-853) was ordered directly from Selleck Chemicals' product catalog, the remaining compounds were synthesized and supplied from WuXi AppTec all at > 90% purity. Compounds were QC'ed internally, resolubilized in DMSO, and diluted to 1 mM and 10 mM working concentrations.

Sample Preparation for MS

$KRAS^{G12C}$ inactive-state protein (produced at Viva Biotech) in stock solution consisting of 50 mM HEPES, 2 mM $MgCl_2$, 100 mM NaCl, 100 μM GDP, and with a resulting pH of 7.4 was diluted to a 0.8 μM protein concentration master mix solution consisting of 25 mM HEPES (Fisher Scientific, NC0470071), 2 mM $MgCl_2$ (Fisher Scientific, 50-983-241), 10 mM NaCl (Fisher Scientific, 50-983-260), 100 μM GDP (Sigma Aldrich, G7127-1G), and with a resulting pH of 7.4.

SKP1-FBWX7 protein complex (produced internally) in stock solution consisting of 50 mM HEPES, 200 mM NaCl, 2 mM TCEP, and with a resulting pH of 6.8, was diluted to a 0.5 μM protein concentration master mix solution in Dulbecco's Phosphate-Buffered Salt

Table 3 | Deconvolution settings for each protein or protein complex used in this study

	$KRAS^{G12C}$	SKP1-FBXW7	SOCS2-EloB-EloC
Mass range (kDa)	10–60	15–55	8–35
Mass step (Da)	1	1	1
m/z range	800–1600	750–3000	700–3000
Time window (minutes)	0.23–0.44	0.215-0.3	0.23-0.4
Peak signal-to-noise	≥ 30	≥ 30	≥ 30
Maximum peak limit by height to the largest	100	100	100
Minimum consecutive charge state	5	5	5
Minimum protein fit score	8	8	8

Solution (Fisher Scientific, MT21031CM). The protein complex was shown to have a purity of at least 90% by SDS-Page and HPLC-SEC.

SOCS2-EloB-EloC protein complex (produced internally) in stock solution consisting of 50 mM HEPES, 250 mM NaCl, 1 mM TCEP, and with a resulting pH of 7.5, was diluted to a 0.5 μM protein concentration master mix solution in Dulbecco's Phosphate-Buffered Salt Solution (Fisher Scientific, MT21031CM). The protein complex was shown to have a purity of at least 90% by SDS-Page and HPLC-SEC.

Compounds were dispensed with an Echo 650 liquid handler into 384-well plates (Fisher Scientific, 07-000-890) at assay concentrations with 3% final DMSO (Fisher Scientific, BP231-100) at concentrations according to Table 1. Protein master mix was added to assay plates at room temperature (22 °C incubator) according to assay time points, and samples were quenched with 4% formic acid (Fisher Scientific, A117-50) solution following incubation. We determined compound solubilities experimentally and generally observed reproducible results and reliable solubility for dose conditions below 400 μM.

Measuring Intact Protein Modification by RapidFire-ToF MS

Samples were analyzed by ESI+ mass spectrometry on an Agilent RapidFire high-throughput MS system connected to an Agilent 6230 Time-of-Flight mass spectrometer. Samples were injected onto a RapidFire™ C8 cartridge for $KRAS^{G12C}$ and a C4 cartridge for SKP1-FBWX7 and SOCS2-EloB-EloC complexes. Samples were eluted into the ToF with the RapidFire settings as follows: pump 1 = 0.4 mL/min, pump 2 = 0.6 mL/min, pump 3 = 0.4 mL/min, aspiration = 400 ms, load = 7000 ms, extra wash = 5000 ms, elute = 10000 ms, re-equilibrate = 700 ms. Furthermore, the source settings were as follows: drying gas temp = 365 °C, drying gas = 12 L/min, VCap = 5550 V, fragmentor = 175 V, nozzle voltage = 2000 V, skimmer = 75 V, nebulizer = 60 psi, capillary = 0.051 μA, sheath gas flow = 12 L/min, sheath gas temp = 400 °C. The instrument was tuned in 3200 m/z mode, 2 GHz, with extended dynamic range. Throughout this study, 832 unique samples were acquired in technical duplicate for a total of 1664 samples.

MS Data analysis

Raw spectra were deconvoluted in Agilent MassHunter Bioconfirm Version 10 software using the Maximum Entropy deconvolution algorithm and settings from Table 3.

Deconvoluted spectra were analyzed for identification of parent and adduct peaks corresponding to specific compound masses and well locations using an in-house proprietary Python-based (version 3.8) analysis package. Exported results were transposed into GraphPad Prism version 10.1.2 for curve-fit generations based on the equations outlined above. The linear regression analysis was also performed in Prism using the Simple Linear Regression built-in analysis.

Kinetic data simulations

Data simulation was performed using KinTek Global Kinetic Explorer version 11.0.1 (KinTek Corp)[26,40]. Full DRTC progress curves were simulated for the two-step irreversible kinetic model:

$$P + L \rightleftharpoons P \times L(k_{on}, k_{off})$$

$$P \times L \rightarrow P - L(k_{inact})$$

where P = protein target, L = covalent modifier, $P \times L$ = noncovalent binary complex, P-L = covalent binary complex. The reversible binding step was treated as a rapid equilibrium, and the rate constant k_{on} was fixed at the diffusion limit ($10^8 M^{-1}s^{-1}$). Datasets were simulated for each individual combination of K_I and k_{inact}/K_I from Supplementary Table 7.

The observable signal (%Modification) was defined as a fraction of the covalent binary complex P-L as follows:

$$\%\text{Modification} = 100\% \times [P - L]/([P] + [P \times L] + [P - L)) \quad (12)$$

The %Modification data points were simulated for the [P] = 0.8 μM and [L] according to **Series 1**: 1.65, 1.65, 3.8, 5.8, 10.9, 25, 57, 85 μM, for 10,800 s, and 15 s interval between points (Table 1). In addition, an analogous dataset was generated for the concentrations according to **Series 2**: 1.56, 3.13, 6.25, 12.5, 25, 50, 100, 200 μM, for 72,000 s, and 60 s interval between points (Table 1). From each full DRTC dataset, the diagonal slices corresponding to the time-concentration combinations in Table 1 were extracted.

For each slice where the simulated signal reached at least 80% modification, %Modification was plotted versus $[L]^{-1}Time^{-1}$ and fitted to the four-parameter logistic nonlinear regression corresponding to the equation: %Modification = 100 + 100 / (1 + (([L]*t)−1 / OC_{50})^Hill), in GraphPad Prism version 10.1.2. Resulting OC_{50} values were converted to estimates of k_{inact}/K_I according to the equation: $k_{inact}/K_I = \ln 2 \times OC_{50}$. The results were summarized in Supplementary Table 7.

Reporting summary

Further information on research design is available in the Nature Portfolio Reporting Summary linked to this article.

Data availability

The authors declare that the data supporting the findings of this study, enabling the recreation of the figures, are available within the paper and its Supplementary Information files. Source data are provided with this paper as a Source Data file. The raw data from the mass spectrometer used in this study are available in the Harvard Dataverse database: https://doi.org/10.7910/DVN/DC3MJH. Source data are provided in this paper.

References

1. Ghosh, A. K., Samanta, I., Mondal, A. & Liu, W. R. Covalent inhibition in drug discovery. *ChemMedChem* **14**, 889–906 (2019).
2. Pan, Z. et al. Discovery of selective irreversible inhibitors for bruton's tyrosine kinase. *ChemMedChem* **2**, 58–61 (2007).

3. Canon, J. et al. The clinical KRAS(G12C) inhibitor AMG 510 drives anti-tumour immunity. *Nature* **575**, 217–223 (2019).
4. Erlanson, D. A. et al. Site-directed ligand discovery. *PNAS* **97**, 9367–9372 (2000).
5. Lanman, B. A. et al. Discovery of a covalent inhibitor of KRASG12C (AMG 510) for the treatment of solid tumors. *J. Med. Chem.* **63**, 52–65 (2020).
6. Ostrem, J. M., Peters, U., Sos, M. L., Wells, J. A. & Shokat, K. M. K-Ras(G12C) inhibitors allosterically control GTP affinity and effector interactions. *Nature* **503**, 548–551 (2013).
7. Shin, Y. et al. Discovery of N-(1-Acryloylazetidin-3-Yl)-2-(1 H-Indol-1-Yl) acetamides as covalent inhibitors of KRASG12C. *ACS Med. Chem. Lett.* **10**, 1302–1308 (2019).
8. Boike, L., Henning, N. J. & Nomura, D. K. Advances in covalent drug discovery. *Nat. Rev. Drug Discov.* **21**, 881–898 (2022).
9. Kathman, S. G., Xu, Z. & Statsyuk, A. V. A fragment-based method to discover irreversible covalent inhibitors of cysteine proteases. *J. Med Chem.* **57**, 4969–4974 (2014).
10. Baltgalvis, K. A. et al. Chemoproteomic discovery of a covalent allosteric inhibitor of WRN helicase. *Nature* **629**, 435–442 (2024).
11. Lucas, S. C. C. et al. Structure-based optimization of a series of covalent, cell active Bfl-1 inhibitors. *J. Med Chem.* **67**, 16455–16479 (2024).
12. Resnick, E. et al. Rapid covalent-probe discovery by electrophile-fragment screening. *J. Am. Chem. Soc.* **141**, 8951–8968 (2019).
13. McLaren, D. G. et al. High-throughput mass spectrometry for hit identification: current landscape and future perspectives. *SLAS Discov.* **26**, 168–191 (2021).
14. Zvonok, N. et al. Covalent inhibitors of human monoacylglycerol lipase: ligand-assisted characterization of the catalytic site by mass spectrometry and mutational analysis. *Chem. Biol.* **15**, 854–862 (2008).
15. Picco, G. et al. Novel WRN helicase inhibitors selectively target microsatellite unstable cancer cells. *Cancer. Discov.* **14**, 1457–1475 (2024).
16. Campuzano, I. D. G. San Miguel, T.; Rowe, T.; Onea, D.; Cee, V. J.; Arvedson, T.; McCarter, J. D. High-Throughput Mass Spectrometric Analysis of Covalent Protein-Inhibitor Adducts for the Discovery of Irreversible Inhibitors. *J. Biomol. Screen.* **21**, 136–144 (2016).
17. Pu, F. et al. High-throughput intact protein analysis for drug discovery using infrared matrix-assisted laser desorption electrospray ionization mass spectrometry. *Anal. Chem.* **94**, 13566–13574 (2022).
18. Strelow, J. M. A Perspective on the kinetics of covalent and irreversible inhibition. *J. Biomol. Screen.* **22**, 3–20 (2017).
19. Bauer, R. A. Covalent inhibitors in drug discovery: from accidental discoveries to avoided liabilities and designed therapies. *Drug Disco. Today* **20**, 1061–1073 (2015).
20. Hopper, M. et al. Relative selectivity of covalent inhibitors requires assessment of inactivation kinetics and cellular occupancy: a case study of ibrutinib and acalabrutinib. *J. Pharmacol. Exp. Ther.* **372**, 331–338 (2020).
21. Craven, G. B. et al. Multiparameter kinetic analysis for covalent fragment optimization by using quantitative irreversible tethering (QIT). *ChemBioChem* **21**, 3417–3422 (2020).
22. Daryaee, F. et al. A quantitative mechanistic PK/PD model directly connects Btk target engagement and in vivo efficacy. *Chem. Sci.* **8**, 3434–3443 (2017).
23. Burt, H. J., Galetin, A. & Houston, J. B. IC50-Based approaches as an alternative method for assessment of time-dependent inhibition of CYP3A4. *Xenobiotica* **40**, 331–343 (2010).
24. U. S. Food and Drug Administration. In vitro drug interaction studies - cytochrome P450 enzyme and transporter mediated drug interactions. *FDA Guidance* **1**, 43 (2020).
25. EMA. Guideline on the investigation of drug interactions. in *European Medicines Agency* (2012).
26. Johnson, K. A., Simpson, Z. B. & Blom, T. Global kinetic explorer: A new computer program for dynamic simulation and fitting of kinetic data. *Anal. Biochem.* **387**, 20–29 (2009).
27. Cokol-Cakmak, M., Bakan, F., Cetiner, S. & Cokol, M. Diagonal method to measure synergy among any number of drugs. *J. Vis. Exp.* e57713 https://doi.org/10.3791/57713 (2018).
28. Cokol, M., Kuru, N., Bicak, E., Larkins-Ford, J. & Aldridge, B. B. Efficient measurement and factorization of high-order drug interactions in mycobacterium tuberculosis. *Sci. Adv.* **3**, e1701881 (2017).
29. Copeland, R. A. Evaluation of enzyme inhibitors in drug discovery. A guide for medicinal chemists and pharmacologists. *Methods Biochem. Anal.* **46**, 1–265 (2005).
30. Hansen, R. et al. The reactivity-driven biochemical mechanism of covalent KRASG12C inhibitors. *Nat. Struct. Mol. Biol.* **25**, 454–462 (2018).
31. Patricelli, M. P. et al. Selective inhibition of oncogenic KRAS output with small molecules targeting the inactive state. *Cancer Discov.* **6**, 316–329 (2016).
32. Petri, L. et al. Size-dependent target engagement of covalent probes. *J. Med. Chem.* **68**, 6616–6632 (2025).
33. Huynh, M. V. et al. Oncogenic KRAS G12C: kinetic and redox characterization of covalent inhibition. *J. Biol. Chem.* **298**, 102186 (2022).
34. Li, K. S. et al. High-throughput kinetic characterization of irreversible covalent inhibitors of KRASG12C by intact protein MS and targeted MRM. *Anal. Chem.* **94**, 1230–1239 (2022).
35. Miyahisa, I., Sameshima, T. & Hixon, M. S. Rapid determination of the specificity constant of irreversible inhibitors (k Inact / K I) by means of an endpoint competition assay. *Angew. Chem.* **127**, 14305–14308 (2015).
36. Mader, L. K. & Keillor, J. W. Fitting of kinact and KI values from endpoint pre-incubation IC50 data. *ACS Med. Chem. Lett.* **15**, 731–738 (2024).
37. Thorarensen, A. et al. The advantages of describing covalent inhibitors in vitro potencies by IC50 at a fixed time point. IC50 determination of covalent inhibitors provides meaningful data to medicinal chemistry for SAR optimization. *Bioorg. Med. Chem.* **29**, 115865 (2021).
38. Obach, R. S. & Walsky, R. L. Venkatakrishnan, K. Mechanism-based inactivation of human cytochrome P450 enzymes and the prediction of drug-drug interactions. *Drug Metab. Dispos.* **35**, 246–255 (2007).
39. Maurer, T. S., Tabrizi-Fard, M. A. & Fung, H.-L. Impact of Mechanism-Based Enzyme Inactivation on Inhibitor Potency: Implications for Rational Drug Discovery. *J. Pharm. Sci.* **89**, 1404–1414 (2000).
40. Johnson, K. A., Simpson, Z. B. & Blom, T. FitSpace explorer: An algorithm to evaluate multidimensional parameter space in fitting kinetic data. *Anal. Biochem.* **387**, 30–41 (2009).
41. Gunnarsson, A. et al. Regenerable biosensors for small-molecule kinetic characterization using SPR. *SLAS Discov.* **26**, 730–739 (2021).

Acknowledgements

The authors would like to thank Kara Herlihy for her careful review and insightful comments, and Evan McMahon, Koli Basu, Courtney Daczkowski, and Weiru Wang for assistance with protein production and Nicole Blaquiere for the design of SKP1-FBXW7 ligands.

Author contributions

J.J. designed experiments, analyzed data and wrote the manuscript, B.H.T. collected and analyzed data and wrote the manuscript, S.A.K. conducted simulations, analyzed data and wrote the manuscript, K.E.M.

and D.A.E. designed experiments and wrote the manuscript, R.A.E. conceived the project, designed experiments, and wrote the manuscript.

Competing interests
The authors declare no competing interests.

Additional information
Supplementary information The online version contains supplementary material available at https://doi.org/10.1038/s41467-025-66924-0.

Correspondence and requests for materials should be addressed to Robert A. Everley.

Peer review information *Nature Communications* thanks Hui Jing, Jon Williams, and the other anonymous reviewers for their contribution to the peer review of this work. A peer review file is available.